

# Theory of magnetic order in $\text{Fe}_{1+y}\text{Te}_{1-x}\text{Se}_x$

CHEN FANG<sup>1</sup>, B. ANDREI BERNEVIG<sup>2</sup> and JIANGPING HU<sup>1</sup>

<sup>1</sup> *Department of Physics, Purdue University - West Lafayette, IN 47907, USA*

<sup>2</sup> *Princeton Center for Theoretical Science, Princeton University - Princeton, NJ 08544, USA*

received 26 January 2009; accepted in final form 25 May 2009  
published online 9 July 2009

PACS 74.25.Ha – Magnetic properties

PACS 71.10.-w – Theories and models of many-electron systems

PACS 71.27.+a – Strongly correlated electron systems; heavy fermions

**Abstract** – We develop a local spin model to explain the rich magnetic structures in the iron-based superconductors  $\text{Fe}_{1+y}\text{Te}_{1-x}\text{Se}_x$ . We show that our model exhibits both commensurate antiferromagnetic and incommensurate magnetic order along the crystal  $a$ -axis. The transition from the commensurate to the incommensurate phase is induced when the concentration of excess Fe atoms is larger than a critical value. Experimentally measurable spin-wave features are calculated, and the mean-field phase diagram of the model is obtained. Our model also suggests the existence of a large quantum critical region due to strong spin frustration upon increasing Se concentration.

Copyright © EPLA, 2009

Superconductivity with critical temperature  $T_c = 14\text{ K}$  was recently reported in the iron-selenide-telluride compound  $\text{Fe}_{1+y}\text{Te}_{1-x}\text{Se}_x$  [1–4] with  $0 \leq x \leq 1$ . This discovery not only adds a new class of iron-based superconductors to the multitude of already existing ones, but also provides a fresh angle to investigate the fundamental physics of the Fe–As-based superconductors [5–8].  $\text{Fe}_{1+y}\text{Te}_{1-x}\text{Se}_x$ , similar to the Fe–As-based materials, has a PbO structure of square planar sheets of tetrahedrally coordinated Fe atoms. The electronic band structure of  $\text{Fe}_{1+y}\text{Te}_{1-x}\text{Se}_x$  calculated by LDA is very close to that of the Fe–As-based superconductors [9]. It exhibits electron pockets at the zone corner and hole pockets at the zone center. Similar to the Fe–As-based superconductors, it is believed that the magnetism in  $\text{Fe}_{1+y}\text{Te}_{1-x}\text{Se}_x$  plays an important role in forming electron Cooper pairs.

The parent compounds of the Fe–As-based superconductors exhibit stripe-type commensurate antiferromagnetic spin order [10]. However, the origin of the spin order has been theoretically controversial, with two very different mechanisms leading to the same physical answer. One theory is based on Fermi surface nesting between the electron and hole pockets at the zone corner and center, respectively [11]. This weak-coupling approach leads to a commensurate spin density wave (SDW) state at the nesting wave vector, as observed in the experiments on Fe–As-based parent materials. The competing view is that, due to the geometry of As-mediated hopping,

antiferromagnetic exchange exists not only between the nearest-neighbor (NN) Fe sites, but also between next-nearest-neighbor (NNN) sites [12–18]. Moreover, the NNN coupling strength  $J_2$  is stronger than the half of the NN coupling strength  $J_1/2$ . The resulting  $J_1$ - $J_2$  model produces magnetic physics consistent with the experimental results. Although they lead to the same overall prediction, the two theories rely on different mechanisms to describe the parent state’s magnetism, and a conclusive test of either of them is needed.

We believe that the recent neutron scattering data in  $\text{Fe}_{1+y}\text{Te}_{1-x}\text{Se}_x$  [19,20] sheds new light on the origin of magnetism in Fe-based materials. A commensurate spin order along the  $a$ -axis (see fig. 1) in FeTe was reported. This gives way to an incommensurate spin order along the same axis upon the introduction of excess Fe atoms. The commensurate spin order in FeTe is different from the one in the Fe–As parent compounds: the two ordered wave vectors are rotated by 45 degrees with respect to each other. This experimental fact places a clear challenge to theories based on Fermi surface nesting. The Fermi surfaces of  $\text{Fe}_{1+y}\text{Te}_{1-x}\text{Se}_x$  are predicted, from LDA studies, to be similar to those in the Fe–As-based materials: the electron and hole pockets are separated by a 2D nesting vector at  $(\pi, 0)$ . Based on first-principle calculations, it was then predicted that FeTe should support an identical spin ground state to that observed in Fe–As materials [9]. With the experiment falsifying

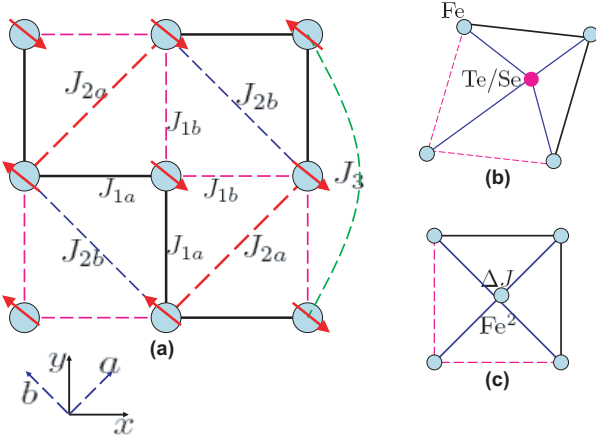


Fig. 1: (Color online) (a) Fe (noted as Fe<sup>1</sup>) square lattice showing commensurate AFM3 order along the  $a$ -axis. The magnetic exchange parameters  $J_{1a}$ ,  $J_{1b}$ ,  $J_{2a}$  and  $J_{2b}$  are specified. (b) The monoclinic lattice distortion observed in neutron scattering [19,20]. (c) The magnetic exchange coupling between Fe<sup>1</sup> and an excess iron atom in the middle of the plaquette indicated as Fe<sup>2</sup>.

this prediction, the spin order in FeTe cannot be, at least trivially, understood by a Fermi surface nesting mechanisms.

In this letter, we show that the magnetic physics in the FeTe parent compound can be understood from the usual magnetic exchange nearest- and next-nearest-neighbor  $J_1$ - $J_2$  model used for the Fe-As-based materials, but with a natural parameter extension that takes into account the monoclinic lattice distortion observed in these compounds. The lattice distortion in Fe<sub>1+y</sub>Te<sub>1-x</sub>Se<sub>x</sub> is different from the one in Fe-As-based materials. The two lattice distortion directions form a 45-degree angle, just like the magnetic wave vectors in the magnetic ordering states of these two systems. Our extended  $J_1$ - $J_2$  model can explain both the commensurate and the incommensurate spin order phases along the  $a$ -axis which have been measured in neutron scattering experiments. The commensurate-to-incommensurate phase transition takes place at a critical concentration of excess Fe atom in Fe<sub>1+y</sub>Te<sub>1-x</sub>Se<sub>x</sub>. Above the critical concentration, the incommensurate wave vector is proportional to the square root of the concentration difference of excess Fe atoms.

We start with the  $J_1$ - $J_2$  model on the tetragonal lattice. Due to their proximity in temperature, we strongly believe that the lattice and magnetic transitions in Fe-based materials are physically related. Considering the coupling between the lattice and magnetism, it is physical to assume that a particular lattice distortion favors changes in the values of  $J_1$  and  $J_2$  as follows: in the Fe-As compounds,  $J_1$  should be slightly more sensitive to changes in the angle of the Fe-As-Fe bond (As is out of plane) than  $J_2$ . This is because the angle between two nearest Fe atoms is around 72 degrees and hence closer to 90 degrees than the one between two next-nearest Fe atoms which is around 112 degrees. However, in

Fe<sub>1+y</sub>Te<sub>1-x</sub>Se<sub>x</sub>,  $J_2$  should be significantly more sensitive than  $J_1$  to changes in the angle between two nearest Fe atoms; the angle between two nearest Fe atoms, which influences  $J_1$ , is around 66 degrees, whereas the angle between the two next-nearest Fe atoms is around 96 degrees and hence much closer to 90 degrees.

In the monoclinic lattice distorted phase, the extended magnetic Hamiltonian can be written as an in-plane nearest- and next-nearest-neighbor Heisenberg model supplemented by an out-of plane small antiferromagnetic coupling as well as a next-next-nearest-neighbor term:

$$H = J_z \sum_{i,n} \vec{S}_i^n \vec{S}_i^{n+1} + \sum_n \sum_{\langle ij \rangle} J_{ij} \vec{S}_i^n \vec{S}_j^n + J_3 \sum_n \sum_{\langle\langle ij \rangle\rangle} \vec{S}_i^n \vec{S}_j^n, \quad (1)$$

where  $n$  is the layer index. The  $J_{ij}$ 's, defined in fig. 1, are the magnetic exchange coupling parameters between irons in the  $a$ - $b$  plane, and their values depend on the lattice distortion direction. If small, the added  $J_3$  next-next-nearest-neighbor coupling, suggested by first-principle calculations [21], influences the phase diagram only quantitatively. We take  $J_{2a} \geq J_{2b}$ ,  $J_{1a} \geq J_{1b}$  and study the part of the phase diagram of the model for which  $(J_{2a}, J_{2b}) > 0$  and  $J_{1a} > 0$ . These values are naturally expected in Fe<sub>1+y</sub>Te<sub>1-x</sub>Se<sub>x</sub>, as shown in fig. 1. Although we have presumed the antiferromagnetic exchange coupling  $J_{1(a,b)}$ , all major results of this work remains unchanged even when the spin exchanges  $J_{1(a,b)}$  flip their signs. As the exchange along the  $c$ -axis  $J_z > 0$  is not frustrated, we only focus on in-plane magnetism. All the possible ground states are presumed to have a  $k_z = \pi$ . The classical ground state of the Hamiltonian can be obtained by comparing the energy of the following six states: 1)  $(\pi, \pi)$  antiferromagnetic (AFM) phase (AFM1 phase) with  $E_1 = -J_{1a} - J_{1b} + J_{2a} + J_{2b} + 2J_3$ ; 2)  $(0, \pi)$  AFM state (AFM2 phase) with  $E_2 = -J_{2a} - J_{2b} + 2J_3$ ; 3) commensurate AFM along the  $a$ -axis (AFM3) with  $E_3 = -J_{1a} - J_{2a} + J_{1b} + J_{2b} - 2J_3$  (see fig. 1); 4) incommensurate AFM along the  $b$ -axis (ICB phase) with energy  $E_4 = -2(J_{2a} + J_3) - \frac{(J_{1a} - J_{1b})^2}{4(J_{2a} + 2J_3)}$ ; 5) incommensurate AFM along the  $a$ -axis (ICA phase) with  $E_5 = \text{Min}(J_{2b} + J_{1a} \cos(\phi_1) + J_{1b} \cos(\phi_2) + (J_{2a} + 2J_3) \cos(\phi_1 + \phi_2))$ , to be minimized with respect to  $\phi_1$  and  $\phi_2$ ; 6) incommensurate AFM along the  $y$ -axis (ICY phase), with  $E_6 = -\frac{J_{1a} + J_{1b}}{2} - J_3 - \frac{(J_{2a} + J_{2b} - (J_{1a} + J_{1b})/2)^2}{4J_3}$ . The three incommensurate phases are depicted in fig. 2.

The phase diagram of above model in the  $\frac{J_{1a}}{J_{2a}} - \frac{J_{1b}}{J_{2a}}$  plane is plotted in fig. 2. For FeTe, we are interested in the AFM3 and ICA phases, which have been experimentally observed. The AFM3 phase exists when the following two conditions are satisfied:  $J_{1a} \geq J_{1b} + 4J_{2b} - 8J_3$  and  $\frac{J_{1b}}{J_{2a}} \leq \frac{J_{1a}}{J_{1a} + J_{2a}^t}$  where  $J_{2a}^t = J_{2a} + 2J_3$ . The transition line between AFM3 and ICA phases is determined by equality in the latter

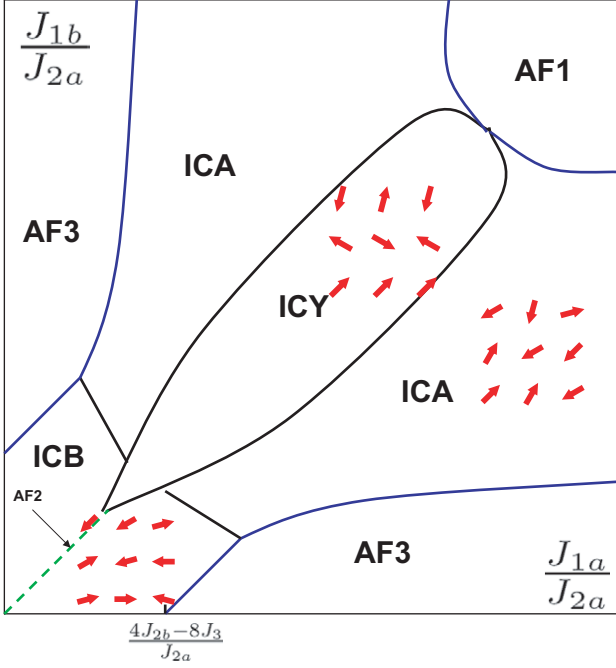


Fig. 2: (Color online) The phase diagram of the  $J_1(J_{1a}, J_{1b})$ - $J_2(J_{2a}, J_{2b})$ - $J_3$  model: 1) AFM1 is the familiar  $(\pi, \pi)$  antiferromagnetic order in a square lattice; 2) AFM2 is the  $(0, \pi)$  collinear AFM order along the  $x$ -axis observed in the Fe-As-based superconductors; it is possible in the present model when  $J_{1a} = J_{1b}$ , indicated as the green line in the figure; 3) AFM3 is the collinear commensurate AFM order along the  $a$ -axis observed in  $\text{Fe}_{1+y}\text{Te}_{1-x}\text{Se}_x$ ; 4) ICB is an incommensurate phase with the incommensurate vector along the  $b$ -axis; 5) ICA is an incommensurate phase with the incommensurate vector along the  $a$ -axis which has been observed in  $\text{Fe}_{1+y}\text{Te}_{1-x}\text{Se}_x$  [19]; 6) ICY is an incommensurate phase that has a wave vector of the form  $(\pi, q)$ .

condition. In the ICA phase, the spin angle difference of two next-nearest-neighbors Fe atoms  $\phi_1$  and  $\phi_2$ , indicated in fig. 2 are given by

$$\cos(\phi_{1,2}) = \mp \frac{J_{2a}^t (J_{1a}^2 - J_{1b}^2 \pm \frac{J_{2a}^2 J_{1b}^2}{(J_{2a}^t)^2})}{2J_{1(a,b)}^2 J_{1(b,a)}}. \quad (2)$$

The incommensurate wave vector,  $\delta$  along the  $a$ -axis corresponding to the definition in [19] is  $\delta = \frac{\phi_1 + \phi_2}{2\pi}$ . If the next-next-nearest-neighbor coupling  $J_3$  is large, its effect on the phase diagram is qualitative. It can be analytically shown that if  $J_3 > J_{2b}/2$ , then the ICB phase disappears; while if  $J_3 > J_{2a}/2$ , then the ICY phase vanishes.

We now phenomenologically justify the parameters  $J_{1a}, J_{1b}, J_{2a}, J_{2b}$  and their capacity to induce a commensurate-incommensurate magnetic order transition upon doping with excess Fe atoms denoted as  $\text{Fe}^2$  (experimentally introduced in FeTe). The excess  $\text{Fe}^2$  atoms are located at the mirror-symmetric site of the Te atom with respect to the Fe layer. This suggests that the additional  $\text{Fe}^2$  directly couples to the four nearest neighbor Fe as shown in fig. 1c with coupling parameter  $\Delta J$ .

In the AFM3 phase, regardless of the sign of  $\Delta J$ , the excess  $\text{Fe}^2$  spins align along the  $b$ -axis through the  $\Delta J$  coupling with the collinear spins along the  $b$ -axis. The  $\Delta J$  coupling along the  $a$ -axis is then frustrated. The effective result of  $\Delta J$  on the magnetic model can be described by changing the effective parameters  $\tilde{J}_{1a}, \tilde{J}_{1b}$  and  $\tilde{J}_{2a}$  as  $\tilde{J}_{1a}(y) = J_{1a} + y\Delta J, \tilde{J}_{1b}(y) = J_{1b} + y\Delta J$  and  $\tilde{J}_{2a}(y) = J_{2a} + y^2\Delta J$ , where  $y$  is the density of the excess Fe atoms. The change of  $J_{2a}$  is of second order in  $y$ , which can be ignored for low concentration of  $\text{Fe}^2$ . According to the phase diagram in fig. 2, the excess Fe atoms can cause a commensurate-incommensurate transition if  $\Delta J$  is antiferromagnetic, *i.e.* positive. From the phase boundary between AFM3 to ICA we can then determine the critical concentration of  $\text{Fe}^2$  that would cause the transition from AFM3 to ICA:

$$y_c = \frac{\sqrt{(J_{1a} - J_{1b})(J_{1a} + 4J_{2a}^t - J_{1b})} - (J_{1a} + J_{1b})}{\Delta J}. \quad (3)$$

Away from the critical concentration, the incommensurate angles as a function  $\delta y = y - y_c$  are given by

$$\cos(\phi_1) = -1 + \frac{2J_{2a}^t + J_{1a}}{J_{2a}^t + J_{1a}} \delta y \Delta J, \quad (4)$$

$$\cos(\phi_2) = 1 - \frac{2(J_{2a}^t)^2 + 3J_{1a}J_{2a}^t + J_{1a}^2}{J_{2a}^t J_{1a}} \delta y \Delta J. \quad (5)$$

Therefore, the incommensurate wave vector close to the transition is given by

$$\delta = \frac{1}{2} - \frac{1}{2\pi} \left( \frac{J_{1a} + J_{2a}^t}{\sqrt{J_{1a}J_{2a}^t}} - 1 \right) \sqrt{\frac{2(J_{1a} + 2J_{2a}^t)\Delta J \delta y}{J_{2a}^t(J_{1a} + J_{2a}^t)}}. \quad (6)$$

As is mentioned previously, the phase diagram given by the model remains unchanged when all the NN exchanges  $J_{1(a,b)}$  flip signs and become FM. This is because, in this *classical* spin model, one can always do the transform that flips all spins on one sublattice, that is, sending  $\vec{S}(i, j)$  to  $-\vec{S}(i, j)$  for  $i + j = \text{odd}$ , which is also the dual transform mapping a ground state for positive  $J_1$ 's to the one for negative  $J_1$ 's without changing its energy. The only formal adaptation is to change the expression of the phase boundaries: for example, changing the boundary between the AFM3 phase and the ICA phase  $\frac{J_{1b}}{J_{2a}^t} = \frac{J_{1a}}{J_{1a} + J_{2a}^t}$  to  $\frac{|J_{1b}|}{J_{2a}^t} = \frac{|J_{1a}|}{|J_{1a}| + J_{2a}^t}$ .

To predict experimentally observable quantities, we perform a spin wave analysis on the AFM3 state. Suppose that the system is in the classical AFM3 ground state, in which the spins are aligned as in fig. 1. This is the commensurate order recently observed in the neutron scattering experiments. By introducing the standard Holstein-Primakoff bosons we obtain the spin wave excitations,

$$H = 2S \sum_{i,j;k} \left[ A_{i,j;k} b_{i,k}^+ b_{j,k} + \frac{B_{i,j;k}}{2} (b_{i,k}^\dagger b_{j,-k}^\dagger + b_{i,-k} b_{j,k}) \right], \quad (7)$$

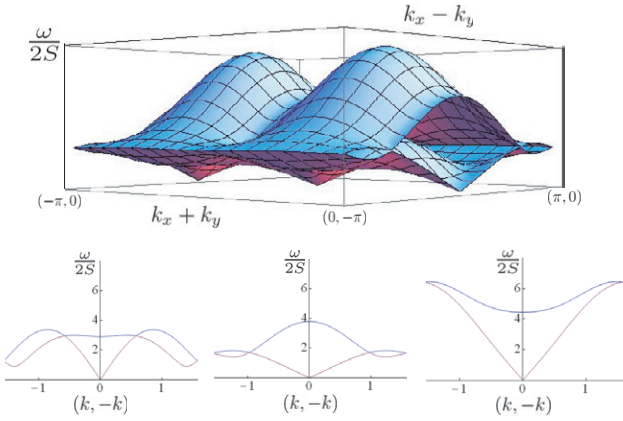


Fig. 3: (Color online) Top: 3D spin wave dispersion for the parameter set of  $J_{2a} = J_{2b} = 1$ ,  $J_{1a} = 2$ ,  $J_{1b} = 0.94$  and  $J_3 = 0.4$ , which gives a point on the AFM3-ICA phase boundary on the phase diagram. Also note that along the BZ boundary ( $k \pm \pi, k$ ), the two sheets are degenerate and almost dispersionless. Bottom: different dispersion at different parameter regions with common parameters  $J_{2a} = J_{2b} = 1$ . All the three dispersions are drawn at AFM3-ICA phase boundary given by (from left to right)  $(J_{1a}, J_{1b}, J_3) = (1, 0.72, 0.8)$ ,  $(J_{1a}, J_{1b}, J_3) = (2, 0.94, 0.4)$  and  $(J_{1a}, J_{1b}, J_3) = (5, 0.9, 0.1)$ , respectively.

where

$$A_k = \begin{pmatrix} \epsilon_1(k) & J_{1b}f(k) \\ J_{1b}f(k)^* & \epsilon_1(k) \end{pmatrix},$$

$$B_k = \begin{pmatrix} \epsilon_2(k) & J_{1a}f(k)^* \\ J_{1a}f(k) & \epsilon_2(k) \end{pmatrix},$$

where  $\epsilon_1(k) = 2(J_{1a} + J_{2a} - J_{1b} - J_{2b} + 2J_3) + 2J_{2b}\cos \times (k_x - k_y)$ ,  $\epsilon_2(k) = 2J_{2a}\cos(k_x + k_y) + 2J_3(\cos(2k_x) + \cos(2k_y))$  and  $f(k) = (e^{ik_x} + e^{ik_y})$ . The explicit analytical expressions for the spin wave dispersion spectra are unreasonably long and will not be given here. We plot the 3D spin wave dispersion in fig. 3. Regardless of the values of parameters, a common feature of the spin wave dispersion is an almost-dispersionless line along  $(k \pm \pi, k)$  where two branches become degenerate with an energy around  $4S\sqrt{(J_{1a} - J_{1b} + 2J_{2a} - 2J_{2b})(J_{1a} - J_{1b} - 2J_{2b} + 4J_3)}$ . By comparing the spin wave dispersions for different  $J_3$ , we can also determine the value of  $J_3$ . In fig. 3, we compare the dispersion along  $(k, -k)$  for  $J_3 = 0.1, 0.4, 0.8$  respectively. The major difference lies in the higher branch, which turns from a convex- to a concave-shaped line. This feature can be tested in inelastic neutron scattering [22] to determine the value of  $J_3$  explicitly.

The spin moment correction in large  $S$  limit is

$$\Delta S = \sum_{i=1,2} \int_{BZ} \langle b_{i,k}^\dagger b_{i,k} \rangle dk^2.$$

In the vicinity of AFM3-ICA transition line,  $\Delta m$  is about 25%. It is worth noting that  $\Delta m$  does not diverge at the phase boundary because the ICA (ICB) phases can be

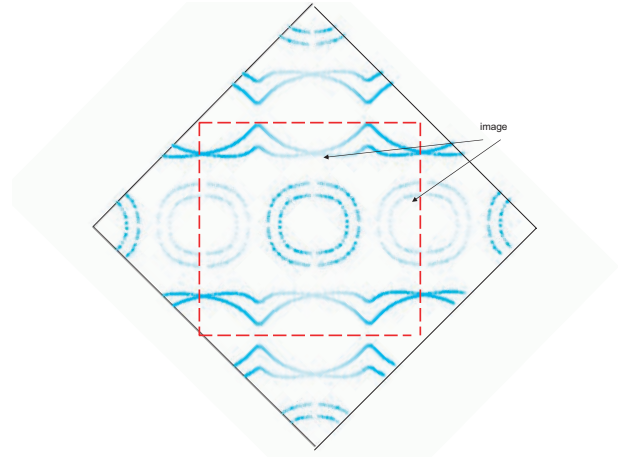
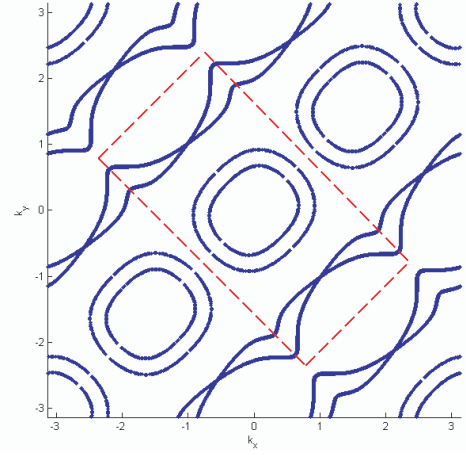


Fig. 4: (Color online) Top: the Fermi surface of the system in the magnetic ordered AFM3 order taking  $A_0 = 0.3t_1$ . The dashed red lines crop out the (folded) Brillouin zone. Bottom: the electronic density of states at the FS with the same parameters, with the dashed lines encircling the experimental FBZ.

obtained from the AFM3 state by a continuous rotation of the magnetization starting from zero at the phase transition line, unlike in other phase transitions where the magnetic order wave vector direction changes [15].

We now discuss the influence of the observed magnetic order in the AFM3 phase on the electronic properties of the material. DFT calculations show that FeSe and FeTe have a very similar Fermi surface structure to that in Fe-As-based materials. In the AFM3 state, the mean-field Hamiltonian can be written as  $H_{mf} = H_0 + H_M$ , where  $H_0 = \sum_{k\sigma} \psi_\sigma^\dagger(k) \epsilon(k) \psi_\sigma(k)$  is kinetic energy that describes the band structure and  $H_M$  is the mean-field energy of the spin ordering,

$$H_M = \sum_{k,q} A(q) (\psi_\uparrow^\dagger(k+q) \psi_\uparrow(k) - \psi_\downarrow^\dagger(k+q) \psi_\downarrow(k)) \quad (8)$$

with  $A(q) = A_0 \sum_{j=0}^1 (1 + i(-1)^j) \delta(q - q_j)$  where  $q_0 = (\frac{\pi}{2}, \frac{\pi}{2})$ ,  $q_1 = (\frac{-\pi}{2}, \frac{-\pi}{2})$  in the AFM3 state. The resulting Fermi surface is given in fig. 4 and remains gapless even at a considerably large order parameter

$A_0 = 0.3t_1$ . The reason is simple: the modulation vector is  $(\pi/2, \pi/2)$ . This vector, and its multiples, can only couple two electron or two hole pockets, but cannot couple electron and hole pockets together. This is in sharp contrast to the 1111 system, where the magnetic order induces a partial gap at both the electron and hole Fermi pockets. To better compare with available ARPES data, we also plotted the electron density at the FS in the SDW state in  $k$ -space (the lower panel of fig. 4). The following features should be noted on this figure: as aforementioned, no gap is seen to open on the Fermi surface; although gapless, the shape of the electron pockets is distorted by the presence of an SDW order; there are “mirror images” of the FS around  $X$  and  $Y$  points of the folded BZ in the SDW state as opposed to zero spectral weight in the normal state. This is because the FS is connected with these regions through the SDW wave vector, thus lending to these regions some spectral weight. The features listed are qualitatively consistent with the experimental data [23].

It is also important to discuss what happens upon replacing Te atoms by Se atoms in the parent compound. Experimentally, it was shown that superconductivity develops in  $\text{FeTe}_{1-x}\text{Se}_x$  upon increasing  $x$ . Based on our model, the AFM3 phase is generated from strong coupling of lattice and magnetic degrees of freedom. The AFM3 phase must coexist with monoclinic lattice distortion which is not favored in the pure  $\alpha$ -FeSe. Therefore, by increasing Se concentration, the magnetic frustration increases. The frustration can lead to a close competition between the AFM3 and AFM2 phases which can result in a strong quantum critical region controlled by a quantum critical point between the AFM3 and AFM2 phases or an existence of a spin liquid state [24], which is an interesting open question to study in future. This physics will be critical to understanding unconventional transport properties in the materials [25] at high temperature or upon increasing the Se concentration.

In summary, we constructed a magnetic exchange model to explain the rich magnetic order in  $\text{Fe}_{1+y}\text{Te}_{1-x}\text{Se}_x$ . The model exhibits both commensurate antiferromagnetic and incommensurate magnetic order along the crystal  $a$ -axis and describes the transition from the commensurate

to the incommensurate spin order upon increasing the concentration of excess Fe atoms. Our model can be explicitly tested by experimentally measurable spin wave features. Our model also suggests an existence of a large critical region due to strong spin frustration upon increasing Se concentration.

\*\*\*

JPH thanks S. KIVELSON, PENGCHENG DAI, IGOR MAZIN, TAO XIANG, Z. Y. LU, WEI BAO, SHILIANG LI, H. YAO, W. TSAI, and D. X. YAO for useful discussions. BAB thanks P. W. ANDERSON and N. P. ONG for useful discussions. JPH and CF were supported by the NSF under grant No. PHY-0603759.

#### REFERENCES

- [1] HSU F.-C. *et al.*, *Proc. Natl. Acad. Sci. U.S.A.*, **105** (2008) 14262.
- [2] YE H. K.-W. *et al.*, arXiv:0808.0474 (2008).
- [3] FANG M. H. *et al.*, *Phys. Rev. B*, **78** (2008) 224503.
- [4] MARGADONNA S. *et al.*, *Chem. Commun.*, **43** (2008) 5607.
- [5] KAMIHARA Y. *et al.*, *J. Am. Chem. Soc.*, **130** (2008) 3296.
- [6] CHEN X. H. *et al.*, *Nature*, **453** (2008) 761.
- [7] CHEN G. F. *et al.*, *Phys. Rev. Lett.*, **100** (2008) 247002.
- [8] WEN H.-H. *et al.*, *EPL*, **82** (2008) 17009.
- [9] SUBEDI A. *et al.*, *Phys. Rev. B*, **78** (2008) 134514.
- [10] DE LA CRUZ C. *et al.*, *Nature*, **453** (2008) 899.
- [11] MAZIN I. I. *et al.*, *Phys. Rev. Lett.*, **101** (2008) 057003.
- [12] YILDIRIM T., *Phys. Rev. Lett.*, **101** (2008) 057010.
- [13] MA F. *et al.*, *Phys. Rev. B*, **78** (2008) 224517.
- [14] SI Q. and ABRAHAMS E., *Phys. Rev. Lett.*, **101** (2008) 076401.
- [15] FANG C. *et al.*, *Phys. Rev. B*, **77** (2008) 224509.
- [16] SEO K. *et al.*, *Phys. Rev. Lett.*, **101** (2008) 206404.
- [17] PARNISH M. M. *et al.*, *Phys. Rev. B*, **78** (2008) 144514.
- [18] XU CENKE *et al.*, *Phys. Rev. B*, **78** (2008) 020501(R).
- [19] BAO W. *et al.*, *Phys. Rev. Lett.*, **102** (2009) 247001.
- [20] LI L. *et al.*, arXiv:0809.0128 (2008).
- [21] MA F. *et al.*, *Phys. Rev. Lett.*, **102** (2009) 177003.
- [22] ZHAO JUN *et al.*, *Phys. Rev. Lett.*, **101** (2008) 167203.
- [23] XIA Y. *et al.*, arXiv:0901.1299 (2009).
- [24] FERRER J., *Phys. Rev. B*, **47** (1993) 8769.
- [25] CHEN G. F. *et al.*, *Phys. Rev. B*, **79** (2009) 140509(R).